Numerical Study of Hydrogen Explosions in a Vehicle Refill Environment

V C Madhav Rao, J X Wen and V H Y Tam
The Centre for Fire and Explosion Studies, Faculty of Engineering, Kingston University
Friars Avenue, London, SW15 3DW, UK

Numerical simulations have been carried out for pressurised hydrogen release through a nozzle in a simulated vehicle refilling environment of an experiment carried out in a joint industry project by Shell, bp, Exxon and the UK HSE, Shirvill[1]. The computational domain mimics the experimental set up for a vertical downwards release in a vehicle refuelling environment. Due to lack of detailed data on pressure decay in the storage cylinder following the release, a simple analytical model has also been developed to provide the transient pressure conditions at nozzle exit. The modelling is carried out using the traditional Computational fluid dynamics (CFD) approach based on Reynolds averaged Navier Stokes equations. The Pseudo diameter approach is used to bypass the shock-laden flow structure in the immediate vicinity of the nozzle. For combustion, the Turbulent Flame Closure (TFC) model is used while the shear stress transport (SST) model is used for turbulence.

Comparison between the predictions and measurement has shown that the predictions have captured the trend of the measured pressure waves but varying degrees of discrepancies exist at some monitoring locations. This is thought to be partly due to the differences in the layout of congestion underneath the car in the computational model and the actual experimental set up due to lack of details in the experimental paper.

The average mass fraction of hydrogen was monitored at the location of sparking which represents the rate at which hydrogen was accumulating in the confined environment. Simulations were carried out for varying and constant mass flow rates through nozzle at different spark timings at 0.5 s, 0.6 s, 0.7 s and 0.8 s after the commencement of release. Comparison was made between the overpressures developed at the various monitoring points to gain insight into pressure wave propagation in confined environments.

Keywords: Hydrogen, high-pressure blowdown release, refill station, pseudo diameter, Turbulent Flame Closure (TFC) model and shear stress transport (SST) model

Nomenclature

d_{eq}	- Equivalent pseudo diameter	(m)
d_j	- Nozzle diameter	(m)
P_e	- Nozzle exit pressure	(MPa)
P	- Pressure	(MPa)
T	- Temperature	(K)
ρ	- Density	(kg/m^3)
R_H	- Hydrogen gas constant	(4124 kJ/kg. K)
Vol	- Volume of storage tank	(m^3)
A_n	- Cross section area of nozzle	(m^2)
a_n	- Sonic velocity	(m/s)
P_t	- Pressure at storage tank	(MPa)

T_t	- Temperature at storage tank	(K)
υ_t	- Specific volume at storage tank	(m^3/kg)
P_n	- Pressure at nozzle exit	(MPa)
T_n	- Temperature at nozzle exit	(K)
υ_n	- Specific volume at nozzle exit	(m^3/kg)
	- Internal energy of hydrogen inside storage tank	(J/kg)
h_t	- Enthalpy of hydrogen inside storage tank	(J/kg)
h_n	- Enthalpy of hydrogen at the nozzle exit	(J/kg)
s	- Entropy	(kJ/kg)
t	- Time	(s)

1. Introduction

Hydrogen as fuel has the highest energy content by mass but the lowest by volume. To have higher energy density, hydrogen is typically stored under higher pressures in comparison to other gaseous fuels. One of the major potential applications of hydrogen is in hydrogen fuel cells vehicles, which could then result in the need for the general public to handle high pressure hydrogen during the refilling process. It is recognised that these hydrogen refill stations would need to have a higher level of safeguards and integrity than those currently used in chemical industries where only a limited number of highly trained personnel are involved. Our work contributes towards the overall understanding of fire and explosion hazards associated with hydrogen transport, and specifically in this paper, the consequences of an accidental release of pressurized hydrogen.

Experiments conducted in different simulated refilling environments [1-3] provide insight of the fire and explosion hazards. The relationship between the overpressures generated and the distance from the source of ignition is importance in determining safe distances e.g. for facility sitting. In the present study, we have firstly carried out numerical studies of the experimentally tested scenarios and then extended the simulations to further investigate the effect of hydrogen release rate and ignition time on the resulting overpressures.

2. Numerical methods

2.1 Pseudo diameter approach

The flow field downstream of a nozzle depends primarily on the ratio of the pressure at the nozzle exit to the ambient pressure. The typical flow through the nozzles at high pressures is choked by critical conditions. A highly underexpanded jet exists at pressure ratios above 2.1 and the flow structure is characterized by the existence of one or more shocks that are normal to the direction of the flow downstream of the nozzle exit [4-5]. Numerical simulations of the shock-containing flow structures require ultra fine computational grids and are extremely time-consuming. Following our previous study of high pressure hydrogen release and the resulting jet flames [4-5], the Pseudo diameter approach is therefore employed to avoid direct computational of the complex shock structures. Instead of the actual nozzle, the flow is assumed to originate from some distance away at an equivalent nozzle diameter. The same mass flow rate is maintained at ambient pressure with sonic velocity conditions

and temperature equal to the exit temperature of the nozzle. Following Birch [6], the pseudo diameter is obtained by the following expression:

$$d_{eq} = d_j \left(\frac{P_e}{P_a} \right)^{0.5} \tag{1}$$

In case of the blow down release considered here, the pseudo diameter varies with release time due to variation of pressure with time at the nozzle throat.

2.2 Analytical model for high pressure hydrogen blowdown release

Analytical model is developed to evaluate the transient properties of hydrogen in the blowdown (constant volume) release. Hydrogen can be approximately treated as an ideal gas up to 172 bar only [7]. At high pressures the real gas effects need to be taken into account and this is considered using the Noble-Able equation of state in the present study,

$$P = \frac{\rho R_H T}{(1 - b\rho)} \tag{2}$$

A series of simultaneous equations describing the thermodynamic relations as developed by Mohamed and Paraschivoiu [8] are then solved using iterative methods starting from the initial stagnation conditions in the storage vessel to evaluate the intermediate states of the hydrogen gas inside the vessel and at the nozzle throat.

The following assumptions were made in deriving the analytical model:

1. A simple configuration for hydrogen release from a convergent nozzle attached to a storage tank is assumed.
2. The thermodynamic properties of the hydrogen gas inside the storage tank are uniform.
3. There is no heat transfer between the gas in storage tank and the surroundings, hence expansion process of hydrogen in the storage tank is adiabatic.
4. Release from the nozzle is choked flow, i.e. nozzle exit velocity is sonic velocity.
5. The hydrogen gas near the nozzle expands isentropically to the critical condition at nozzle exit (sonic condition).
6. Kinetic energy of the hydrogen gas in the storage tank is negligible.

On the basis of the above assumptions, the following equations can be obtained:

The conservation of mass for hydrogen gas inside the tank

$$\frac{\partial \upsilon_t}{\partial t} = \frac{\upsilon_t^2}{V} \frac{a_n A_n}{\upsilon_n} \tag{3}$$

The conservation of energy for the hydrogen gas inside the tank,

$$\frac{\partial i_t}{\partial t} = \frac{i_t \upsilon_t}{Vol} \frac{a_n A_n}{\upsilon_n} - \frac{(h_n + 0.5 a_n^2) a_n A_n}{\upsilon_n} \frac{\upsilon_t}{Vol} \tag{4}$$

The sonic velocity, *a*, is given as

$$a_n = \sqrt{-\upsilon^2 \frac{c_p}{c_\upsilon} \frac{(\partial P/\partial T)_\upsilon}{(\partial \upsilon/\partial T)_p}} = \sqrt{-\upsilon^2 \frac{c_p}{c_\upsilon}\left(\frac{\partial P}{\partial \upsilon}\right)_T} \qquad (5)$$

Following Van et al. [9], the specific internal energy of hydrogen as a real gas is given as:

$$di = c_\upsilon dT + \left[T\left(\frac{\partial P}{\partial T}\right)_\upsilon - P\right] d\upsilon \qquad (6)$$

Integrating equation (6), the specific internal energy is given as,

$$i(T,\upsilon) = \tilde{c}_\upsilon T + \int_{\upsilon_0}^{\upsilon}\left[T\left(\frac{\partial P}{\partial T}\right)_\upsilon - P\right] d\upsilon \qquad (7)$$

From the definition of enthalpy, the specific enthalpy of hydrogen as a real gas is the function of temperature and specific volume given as:

$$h(T,\upsilon) = i(T,\upsilon) + \upsilon P \qquad (8)$$

Substituting eq.8 in the above equation we get,

$$i(T_t,\upsilon_t) + \upsilon_t P_t = i(T_n,\upsilon_n) + \upsilon_n P_n + \frac{1}{2} a_n^2 (T_n,\upsilon_n) \qquad (9)$$

The sonic state of the flow at the nozzle exit is evaluated by satisfying the above equation.

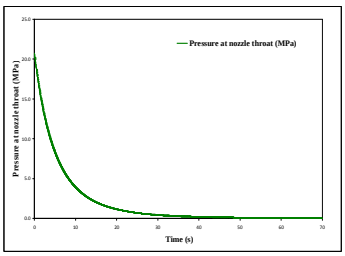

Fig 1. Pressure at nozzle throat

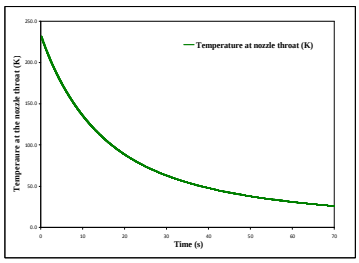

Fig 2. Temperature at nozzle throat

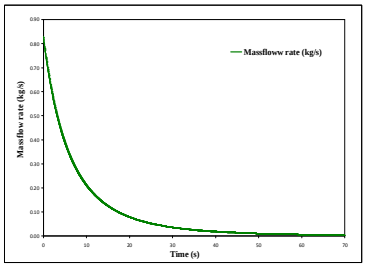

Fig. 3 Blowdown mass flow rate

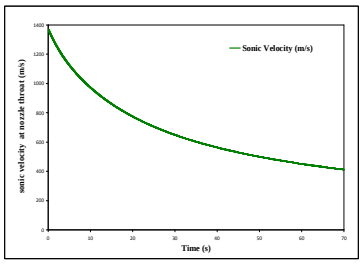

Fig. 4 Sonic velocity at nozzle throat

A computer program is developed to solve the above mentioned isentropic release followed by adiabatic expansion processes iteratively to obtain the blowdown properties of high pressure hydrogen release. The hydrogen blowdown properties at the nozzle exit are plotted in Figs. 1 – 4 for the

following input parameters which were the initial conditions of the compressed cylinder in the experiment:

1) Initial stagnation Pressure in the storage tank = 40.17 MPa
2) Initial stagnation Temperature in the storage tank = 289.4 K
3) Volume of the storage tank = 0.252 m^3
4) Time step of integration = 1.0E-5 s
5) Nozzle diameter = 8 mm
6) Discharge coefficient = 0.75

2.3 Turbulent Flame Closure (TFC) model

The Turbulent Flame Closure (TFC) approach is used to model partially-premixed combustion. This model is also referred as Burning Velocity Model (BVM) in the literature. It solves an additional transport equation for reaction progress variable (c):

$$\frac{\partial}{\partial t}(\overline{\rho c}) + \frac{\partial}{\partial x_k}(\overline{\rho}\,\overline{u}_k\overline{c}) = \frac{\partial}{\partial x_k}\left(\overline{\rho} D_t \frac{\partial \overline{c}}{\partial x_k}\right) + (\rho_u U_t)|\,grad\,\overline{c}\,| \qquad (10)$$

where, $\overline{c} = (\frac{\rho_b}{\overline{\rho}})P_b$ and $\overline{\rho} = \rho_u P_u + \rho_b P_b$

The TFC model is used to close the combustion source term for reaction progress, the closure developed by Zimont [10] is used for the turbulent burning velocity, which is given below

$$s_t = AG u'^{3/4} s_L^{1/2} \lambda_u^{-1/4} l_t^{4} \qquad (11)$$

where A is the modeling coefficient. For H_2/air mixture, it is equal to 0.6 [11]. The stretching factor G, accounts for reduction of the flame velocity due to large strain rate. This effect is modeled in terms of the probability for turbulence eddy dissipation, ε, being larger than a critical value ε_{cr}. For $\varepsilon > \varepsilon_{cr}$ flamelet extinction takes place, while for $\varepsilon < \varepsilon_{cr}$ the stretching effect is completely ignored. Assuming a log normal distribution for ε, the stretching factor is given by

$$G = \frac{1}{2} erfc\left[-\frac{1}{\sqrt{2\sigma}}\left(\ln(\varepsilon_{cr}/\tilde{\varepsilon}) + \frac{\sigma}{2}\right)\right] \qquad (12)$$

where *erfc* denotes the complimentary error function and $\sigma = \mu_{str} \ln(l_t/\eta)$ is the standard deviation of the distribution of ε with μ_{str} being an empirical model coefficient. λ_u is the thermal conductivity of the unburned mixture. The turbulent flame speed closure model is completed with the following models for integral velocity fluctuations level, integral turbulent length scale, and Kolmogorov length scale as given below.

$$u' = \sqrt{2k/3},\ l_t = k^{2/3}/\varepsilon,\ \eta = v^{3/4}/\varepsilon^{1/4}$$

The critical dissipation rate ε_{cr} is computed from a specified critical velocity gradient g_{cr}, and the kinematic viscosity of the fluid ν, according to

$$\varepsilon_{cr} = 15\nu g_{cr}^{2} \qquad (13)$$

The model constants used in the present numerical simulation for the turbulent flame speed closure model are

$$\sigma_c = 0.9, \quad A = 0.65, \quad \mu_{str} = 0.28, \quad g_{cr} = 8000\, s^{-1}$$

The laminar burring velocity s_l is modelled using the equivalence ratio correlation developed by Metghalchi and Keck [9]. Laminar burning velocity is expressed as a base value at reference condition $s_{L,0}$, multiplied by correction factor for preheat and pressure dependencies.

$$s_L = s_{L,0}\left(\frac{T_u}{T_{ref}}\right)^{\alpha}\left(\frac{p}{p_{ref}}\right)^{\beta} \qquad (14)$$

The reference burning velocity $s_{L,0}$ is specified as a fifth order polynomial as given below

$$s_{L,0} = s_0 + s_1\phi + s_2\phi^2 + s_3\phi^3 + s_4\phi^4 + s_5\phi^5$$

The above polynomial is evaluated on a specified fit range, outside the range the burning velocity is modelled to decay linearly to zero at the flammability limits [12].

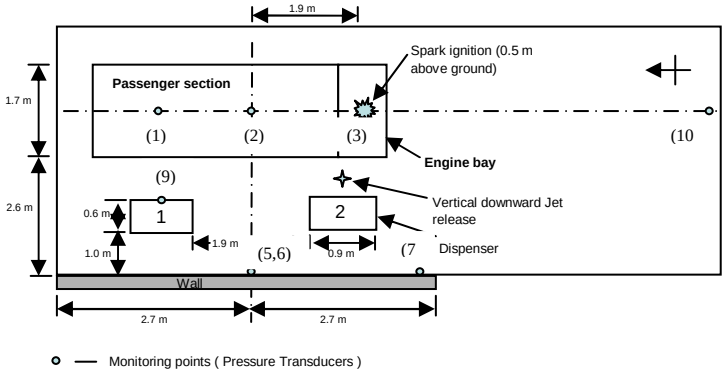

Fig. 5 Schematic layout of the refilling station congestion

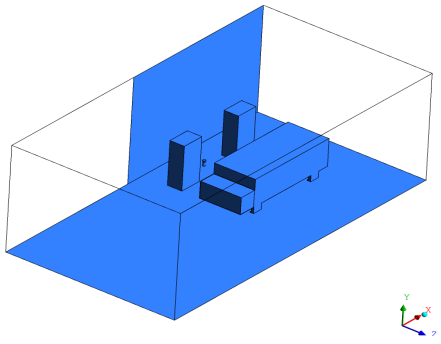

Fig. 6 The computational domain

3. Numerical setup

The congestion at the refuelling station is simulated with a confining wall, two dispensers and a vehicle as shown in Fig. 5 and 6 where the monitoring points are also denoted [10]. The dispenser is 0.6(W)×0.9 (L)×2.1(H) m. The vehicle 'passenger' section is 1.7 (W)×3.8 (L)×1.3(H) m the and 'engine bay' section is 1.7 (W)×0.7 (L)×0.8(H) m. The engine bay is open at the bottom while the 'passenger' section is closed on all sides. The ambient conditions are taken as 1 atm pressure and 290K temperature and the wind speed is 3.7 m/s at 24° northwest direction. The locations of the monitoring points (pressure transducers) for the over pressure are listed in Table 1.

The jet release from the dispenser nozzle is 1.2 m above the ground and directed vertically downwards between the 'engine bay' and the 2nd dispenser. The hydrogen release rate was calculated from the experiments. Apart from the varying mass flow rate, simulations were also conducted at constant flow rate of 2.62 kg/s based on the total mass and time of release used in the experiments [1]. This is thought to be representative of constant discharge pressure at the dispenser nozzle of a refuelling station where hydrogen storage is in a large tank with mechanism to maintain constant supply pressure. The computational domain, shown in Fig. 8, is 15×(L) ×10(W) ×6(H) m.

Table 1 Monitoring point locations

Monitoring point No.	Height above ground (m)	Distance from centre of vehicle (m)
1	0.08	-1.50
2	0.08	0
3	0.08	1.90
10	1.25	6.70
	Height above ground (m)	Distance from centre of wall (m)
4	4.2	0
6	0.08	0
5	2.10	0
7	1.25	2.6
9	On Dispenser	1.25

The Shear Stress Transport (SST) model, which is a combination of K-ε and K-ω model with provision to switch between the two models, i.e. near the wall to K-ω and in the bulk flow to K-ε, is used for turbulence. Opening boundary conditions are applied to the top and lateral sides of the domain. Surface of the confining wall, dispenser and the vehicle are assumed to be as adiabatic free slip wall. The dispenser nozzle is considered as supersonic inlet. High pressure hydrogen jet release is simulated using pseudo diameter approach as discussed in section 2. The blowdown properties shown in Figs. 1-4 are applied at the nozzle exit using the temperature, sonic velocity and pseudo diameter

Ignition of the jet is initiated with a spark, located at the centre of the engine bay and 0.5 m above the ground shown in Fig. 5. Sparking was attempted at 0.5, 0.6, 0.7 and 0.8 s following jet release with spark energy of 50 mJ.

4. Results and discussion

Over Pressure measured at the respective monitoring points during the numerical simulation are plotted for different spark timings. X-axis in the plots represents the time from the initiation of the hydrogen release in each cases. Y-axis of the plot represents the overpressure generated in kPa. The monitoring point 1, 2 and 3 are under the vehicle, with monitoring point 3 being right under the sparking location. The monitoring points 4, 5, 6, 7 and 9 are on the wall and dispenser at the elevations given in table 1.

4.1 Blow down jet release

The mass fraction of the hydrogen at the location of the up to the sparking is shown in Fig.9. Rate of increase of hydrogen mass fraction increased rapidly at the start of release and then gradually reduced with time. Reduction in the hydrogen mass faction in the later part is due to the mixing and dispersion. After uniformity is reached the hydrogen mass fraction picks up once again.

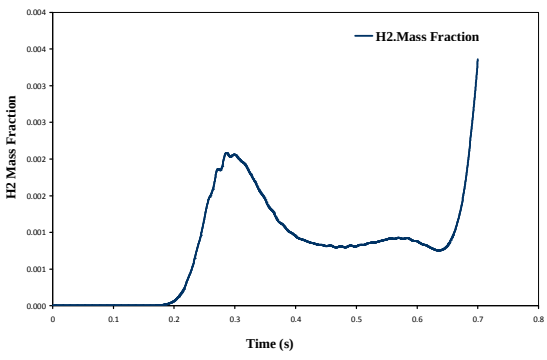

Sparking at 0.5 s and 0.6 s for the blowdown release failed to ignite the hydrogen-air mixture at spark location thought to be due to insufficient mixing which resulted in the hydrogen-air mixture at spark location being too lean at these moments.

Fig. 7 Hydrogen mass fraction at spark location

The pressure wave measured for the 0.7 s sparking at the monitoring points parallel to the wall and on the wall and dispenser are shown in Figs. 8(a) to (i) along with the measurements in [10], which were also for blowdown release ignited at 0.7 s. The data were extracted by digitizing the published results. Shirvill et al. [10] did point out that the timing on the x-axis for the measured pressure curves were adjusted for analysing the results and hence they did not represent the actual time. For the purpose of comparison, we plotted the experimental data in such a way that the locations of peak overpressure are overlapping with the peaks in the predictions.

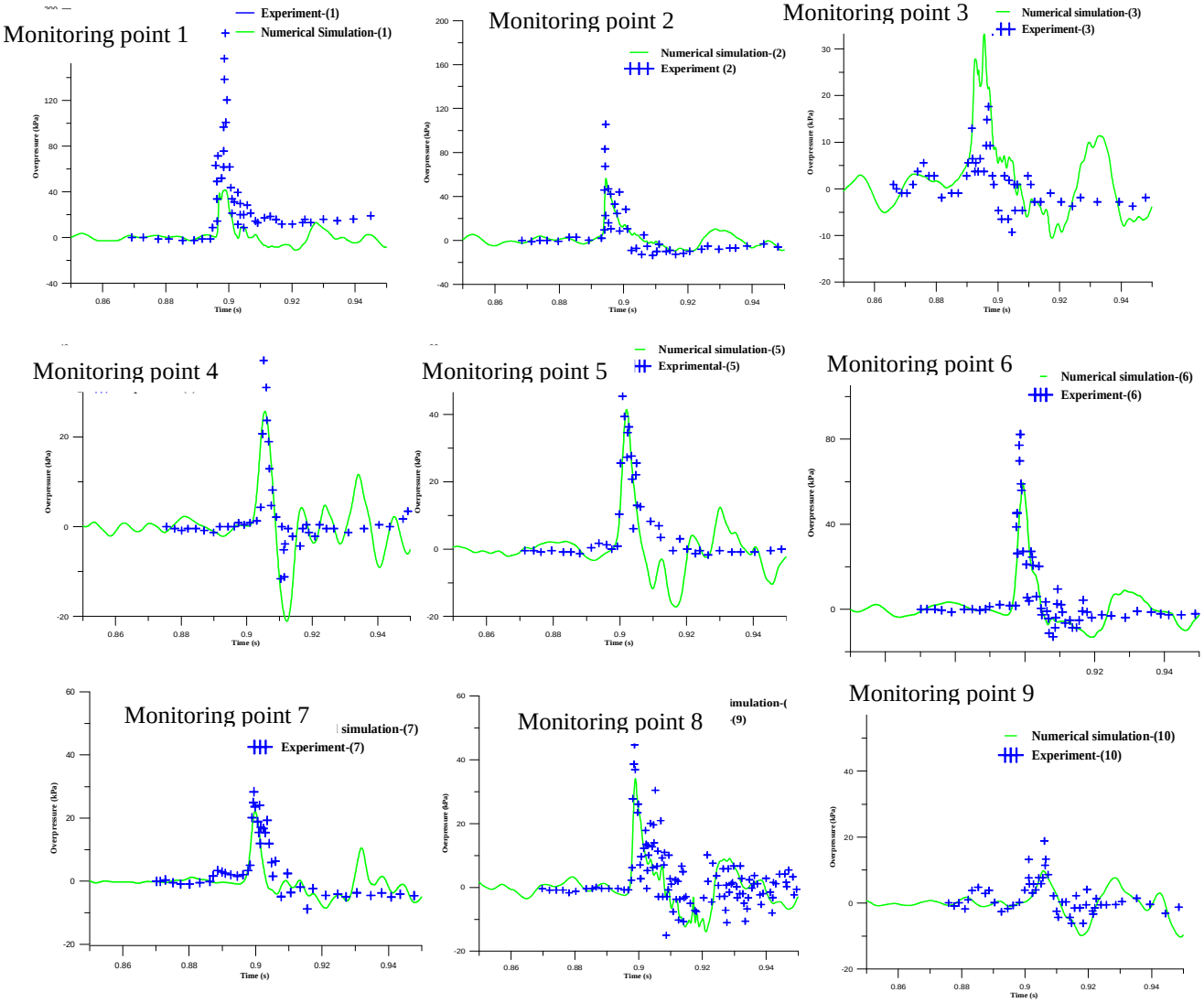

Fig. 8 Comparison of predicted and measured pressure at the monitoring points

It can be seen that the predictions have captured the trend of the measured pressure curves however there are discrepancies in the actual values. Figure shows the comparison for the maximum overpressure obtained in parallel to wall while the comparison for monitoring points on the wall and

dispenser are summarized in Table 2. It can be seen that there are significant differences between the predicted and measured overpressures for monitoring points underneath the vehicle and they are in reasonable agreement for those monitoring points outside the vehicle region.

The overpressure under the vehicle and at the centre (monitoring point 2) is peak due to higher hydrogen concentration and flame acceleration in the confinement. The overpressures generated are directly related to hydrogen concentration in a given system, evident from the published results of Tanaka et. al [3]. The deviation in the numerical simulation results indicate that the hydrogen concentration field under the vehicle is not similar to the one obtained in the experiments.

Table 2 Comparison of predicted and measured overpresures on wall and dispenser

Monitoring points	Distance from wall (m)	Height (m)	Measured [1] (kPa)	Predicted (kPa)	Percentage error
6	0	0.08	86.8	60.1	30.7
5	0	2.10	52.0	41.5	20.1
4	0	4.2	37.0	25.7	30.5
7	2.6	1.25	26.4	22.1	16.2
9	On dispenser	1.25	54.4	36.2	33.4

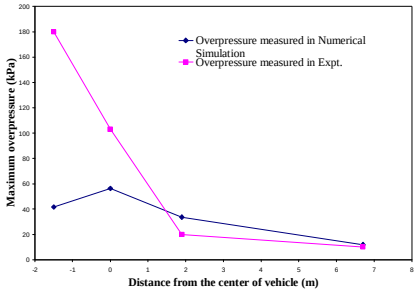

Fig. 9 Comparison of the predicted and measured overpressure parallel to the wall for 0.7 s sparking

It is thought that the main reasons for the above discrepancy for monitoring points underneath the car is due to the uncertainty of the location and size of the L-braced section which supported the vehicle assembly 0.3m above the ground in the experimental setup. As no details were given in [1], we approximated this in the computational set up.

As shown in Fig. 10, one of these L-braced sections is just next to the jet release location and is bifurcating the hydrogen gas flow under the vehicle. Difference in the geometric details of the L-braced supporting section could lead to different hydrogen concentrations underneath the vehicle and hence different explosion overpressure. In addition, the blowdown mass flow rate used in the numerical simulation is based on the prediction of the simple analytical model described in section 2 without considering the flow devices such as stagnation chamber and throttle valves in the path of jet release. There could also be some mismatch in the blowdown mass flow rate.

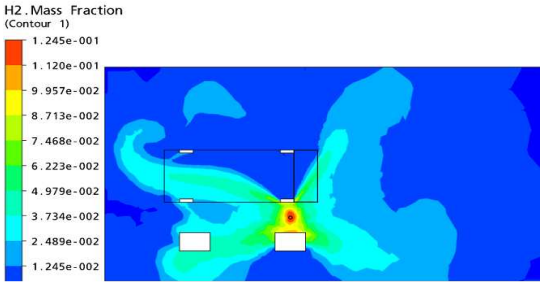

Fig.10 The predicted hydrogen concentration underneath the vehicle

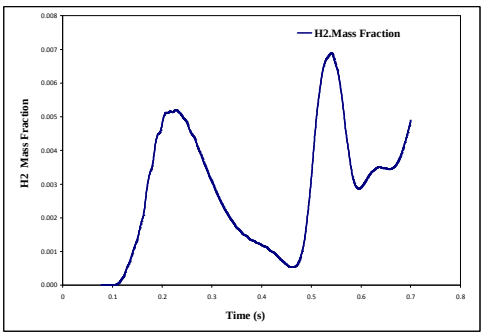

Fig.11 Hydrogen mass fraction at spark location

4.2 Constant flow rate jet release

The mass fraction of hydrogen at spark location up to 0.7 s is shown in Fig. 11. The trend is similar to the blowdown release but the magnitudes are higher due to the constant flow rate.

The predicted overpressure at the monitoring points parallel to the wall and on the wall and dispenser for sparking at 0.5 s after release are shown in Figs. 12 (a) and (b). Those for sparking at 0.6, 0.7 and 0.8 s are shown in Figs. 13 to 15 respectively.

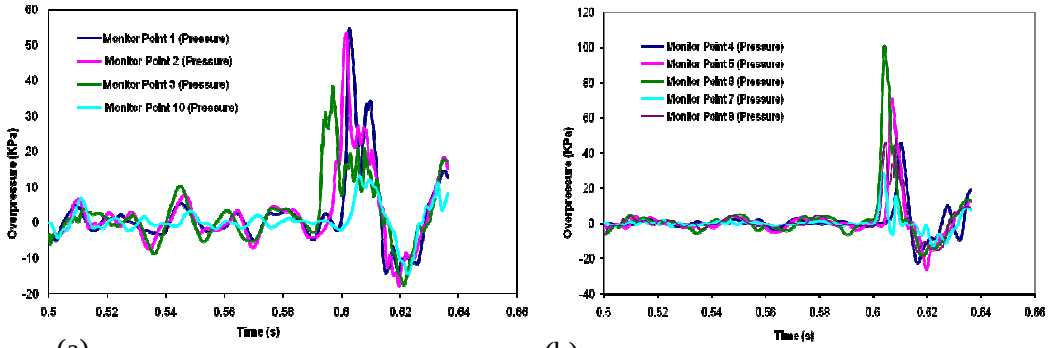

(a) (b)

Fig. 12 The predicted overpressure for sparking at 0.5 s (a) parallel to the wall (b) on the wall and dispenser

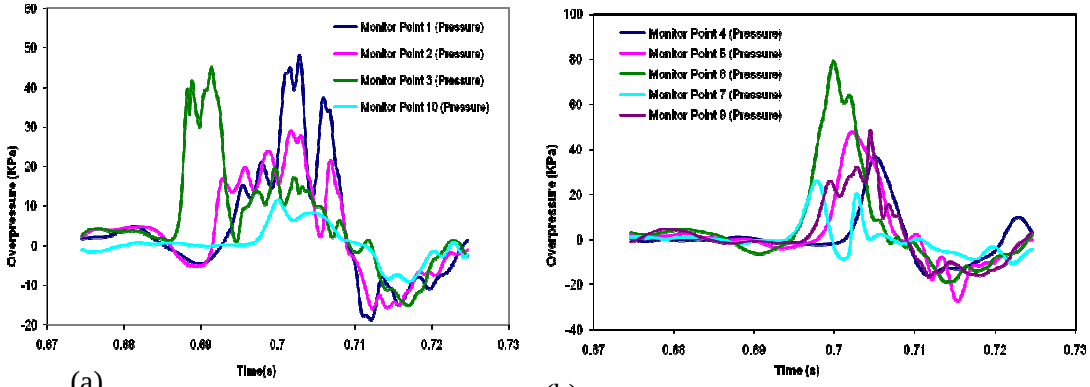

(a) (b)

Fig. 13 The predicted overpressure for sparking at 0.6 s (a) parallel to the wall (b) on the wall and dispenser

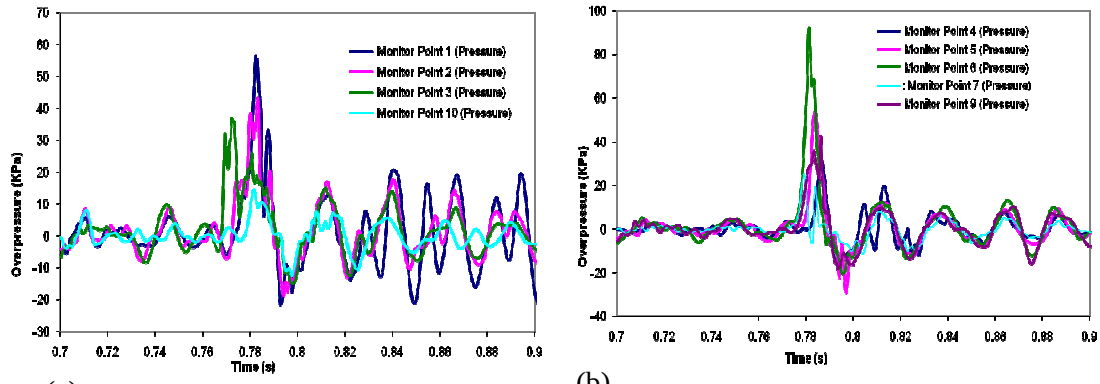

(a) (b)

Fig. 14 The predicted overpressure for sparking at 0.7 s (a) parallel to the wall (b) on the wall and dispenser

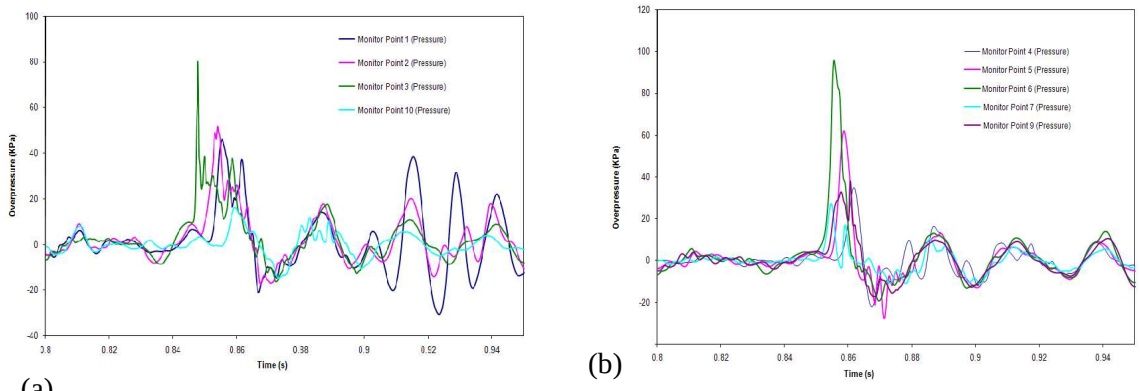

(a) (b)

Fig. 15 The predicted overpressure for sparking at 0.7 s (a) parallel to the wall (b) on the wall and dispenser

Variation of the predicted overpressures shown in Figs. 12 to 15 indicates that while for different ignition time, there is little change in the overpressure on the monitoring points away from the vehicle, the overpressure underneath the vehicle increases with the delayed sparking time. Comparison of the overpressure parallel to the wall for different sparking in Fig. 16 shows that the sparking at 0.8s led to the highest overpressures. This is due to the longer time available for better mixing of hydrogen and air and also the mass of hydrogen released is more. The maximum overpressure was at the location of monitoring point 3 (under the engine bay) for the different spark timings.

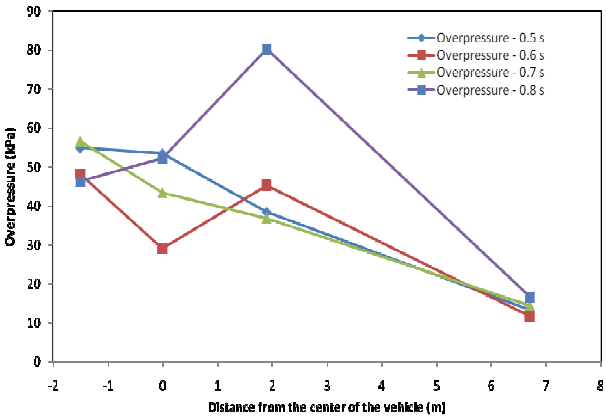

Fig. 16 Comparison of the overpressure parallel to the wall for different sparking time

Conclusions

Numerical simulations have been carried out for pressurised hydrogen release through a nozzle in a congested vehicle refilling environment. Comparison between the predictions and measurement has shown that the predictions have captured the trend of the measured pressure waves but varying degrees of discrepancies exist at some monitoring locations. This is thought to be partly due to the differences in the layout of congestion underneath the car in the computational model and the actual experimental set up due to lack of details in the experimental paper.

The overpressures developed in case of constant mass release are found to be much higher than the blowdown release scenario for the same given total mass. The maximum overpressure generated were under the ‘passenger bay’ for up to 0.7 s sparking and was under the ‘engine bay’ for 0.8 s sparking. This is due to higher hydrogen gas accumulation in the confinement of the engine bay after 0.8 s of

release. The results indicate that little time is required for the released gas to accumulate and form an explosive mixture and importance of reducing unnecessary congestion in a refill environment.

The study has also demonstrated that CFD techniques can act as a useful tool for assessing explosion hazards in refill stations with varying degree of congestion.

Acknowledgments
The authors would like to acknowledge EU FP6 Marie Curie programme for funding hydrogen research at Kingston University through the HYFIRE (Hydrogen combustion in the context of fire and explosion safety) project. We also acknowledge BP and HSL for acting as supporting groups for HYFIRE.

References

1. Shirvill, L.C., Royle, M. and Roberts, T.A., Hydrogen release ignited in a simulated vehicle refuelling environment, *Proc. 2nd Int Conf on Hydrogen Safety, Sep. 11-13, 2007, San Sebastian, Spain*
2. K. Takeno, K. Okabayashi, A. Kouchi, T. Nonaka, K. Hashiguchi, K. Chitose, Dispersion and explosion field tests for 40 MPa pressurized hydrogen, *International Journal of Hydrogen Energy, Volume 32, Issue 13, September 2007, Pages 2144-2153.*
3. T. Tanaka, T. Azuma, J.A. Evans, P.M. Cronin, D.M. Johnson, R.P. Cleaver, Experimental study on hydrogen explosions in a full-scale hydrogen filling station model, *International Journal of Hydrogen Energy, Volume 32, Issue 13, September 2007, Pages 2162-2170*.
4. Zhang, J., Dembele, S. and Wen J. X., Exploratory Study of Under-expanded Sonic Hydrogen Jets and the Resulting Jet Flames, *5th International Seminar on Fire and Explosion Hazards, April 2007, Edinburgh, UK.*
5. B P Xu, J P Zhang, J X Wen, S Dembele and J Karwatzki, Numrerical Study of a Highly Under-Expanded Hydrogen Jet, *Proc. 1st International Conference on Hydrogen Safety, 08-10 September 2005, Pisa, Italy.*
6. A. D. Birch, D. J. Hughes, F. Swaffield, Velocity decay of high pressure jets, *Combustion Science and Technology, 1987, Vol. 52, pp. 161-171*.
7. R. W. Schefer, W.G. Houf, T.C. Williams, B. Bourne, J. Colton, Characterization of high-pressure, underexpanded hydrogen-jet flames, *International Journal of Hydrogen Energy 32, 2007, pages 2081-2093.*
8. Kaveh Mohamed, Marius Paraschivoiu, Real gas simulation of hydrogen release from a high-pressure chamber, *International Journal of Hydrogen Energy 30, 2005, pages 903-912.*
9. Van Wylen G., Sonntag R., Borgnakke C., Fundamentals of classical thermodynamics, 4nd ed, New York, Wiley, 1994.
10. V. L. Zimont, Gas premixed combustion at high turbulence, Turbulent flame closure combustion model, *Experimental thermal and fluid science 21 (2000) 179-186.*
11. Vladimir L. Zimont, Fernando Biagioli, Khawar Syed, Modelling turbulent premixed combustion in the intermediate steady propagation regime, *Progess in computational fluid dynamics, Volume 1, Nos 1/2/3, 2001.*
12. Mohamad Metghalchi, James C. Keck , 1982, Burning velocities of mixtures of air with methanol, isooctane, and indolene at high pressure and temperature Combustion and Flame, Volume 48, Pages 191-210.